# Symmetrical Bisbenzimidazoles with Benzenediyl Spacer: The Role of the Shape of the Ligand on the Stabilization and Structural Alterations in Telomeric G-Quadruplex DNA and Telomer...

**ARTICLE** *in* BIOCONJUGATE CHEMISTRY · JULY 2010

Impact Factor: 4.51 · DOI: 10.1021/bc9003298 · Source: PubMed



**4 AUTHORS**, INCLUDING:

Santanu Bhattacharya
Indian Institute of Science
**238** PUBLICATIONS **6,676** CITATIONS
SEE PROFILE

Akash Jain
Indian Institute of Science
**17** PUBLICATIONS **280** CITATIONS
SEE PROFILE

Ananya Paul
Georgia State University
**14** PUBLICATIONS **189** CITATIONS
SEE PROFILE

# Symmetrical Bisbenzimidazoles with Benzenediyl Spacer: The Role of the Shape of the Ligand on the Stabilization and Structural Alterations in Telomeric G-Quadruplex DNA and Telomerase Inhibition

Santanu Bhattacharya,*[,†,‡] Padmaparna Chaudhuri,[†] Akash K. Jain,[†] and Ananya Paul[†]

Department of Organic Chemistry, Indian Institute of Science, Bangalore 560 012, India, and Chemical Biology Unit, Jawaharlal Nehru Centre for Advanced Scientific Research, Bangalore 560 012, India. Received July 25, 2009; Revised Manuscript Received December 31, 2009

The extremities of chromosomes end in a G-rich single-stranded overhang that has been implicated in the onset of the replicate senescence. The repeated sequence forming a G-overhang is able to adopt a four-stranded DNA structure called G-quadruplex, which is a poor substrate for the enzyme telomerase. Small molecule based ligands that selectively stabilize the telomeric G-quadruplex DNA, induce telomere shortening eventually leading to cell death. Herein, we have investigated the G-quadruplex DNA interaction with two isomeric bisbenzimidazole-based compounds that differ in terms of shape (V-shaped angular vs linear). While the linear isomer induced some stabilization of the intramolecular G-quadruplex structure generated in the presence of $Na^+$, the other, having V-shaped central planar core, caused a dramatic structural alteration of the latter, above a threshold concentration. This transition was evident from the pronounced changes observed in the circular dichroism spectra and from the gel mobility shift assay involving the G-quadruplex DNA. Notably, this angular isomer could also induce the G-quadruplex formation in the absence of any added cation. The ligand−quadruplex complexes were investigated by computational molecular modeling, providing further information on structure−activity relationships. Finally, TRAP (telomerase repeat amplification protocol) experiments demonstrated that the angular isomer is selective toward the inhibition of telomerase activity.

## INTRODUCTION

Telomeres are the noncoding regions of DNA at the end of the chromosomes (*1*). Their function is to counterbalance the function of the chromosome ends that occur with each replication cycle, and this prevents aberrant recombination and degradation by exonucleases (*2*). These are composed of tandem repeats of short G-rich sequences, as exemplified by the 5′-TTAGGG-3′ in human telomeric sequence. With the help of enzyme telomerase, a ribonucleoprotein, the cells are easily replicated indefinitely with reverse transcriptase activity. Telomerase is overexpressed in 85−90% of all cancer cells (*3–5*). Telomerase is therefore a potentially highly selective target for chemotherapeutic intervention cancer chemotherapy (*6, 7*).

Guanine-rich DNA sequence has the ability to form four-stranded inter- and intramolecular guanine quadruplex structures under high salt conditions. Since RNA template of telomerase requires a nonfolded telomeric DNA primer in order to affect telomere synthesis, the formation and the stabilization of G quadruplex structures results in the negative regulation of the telomerase function. To date, a number of families of compounds have been identified and their interactions with G-quadruplex have been extensively studied (*8, 9*), of which a few of them are in clinical use (*10, 11*).

G4 DNAs have several distinct structural features compared with duplex DNA, notably the possession of four quasi-equivalent grooves and a pronounced channel of negative electrostatic potential running through the center of the planes of the G-quate allowing metal ion to be coordinated between the planes in a bipyramidal antipoismatic manner (*12*). Due to these special features, a selective recognition of G-quadruplex by small molecule is possible (*13–15*). So, the design of new G-quadruplex stabilizing ligands involves an attractive strategy to develop new anticancer agents. Typical G-quadruplex binding ligands have planar aromatic molecules, capable of inducing interaction with guanine tetrads via $\pi-\pi$ interactions and also have side chains directed toward the quadruplex loops (*16, 17*). Certain triazole (*18*), indole (*19*), benzimidazole (*20*) and bisquinolinium (*21*) compounds having these properties have been tested.

We have previously reported duplex DNA binding (*22*−*24*), DNA cleaving (*25*−*28*) and DNA-dependent topoisomerase inhibiting properties (*29*). We have also reported the effect of symmetric benzimidazoles on the stability and topology of quadruplex DNA made from *Tetrahymena thermophilla* (*30*). These molecules were derived from 1,3-substituted symmetrical phenylene bisbenzimidazole system and exerted significant influence on the stability of quadruplex DNA depending on the nature of substitution on the aromatic skeleton.

A few G-quadruplex stabilizing small molecules have been designed and investigated, and it was found that isomers which differ in shape and geometry have different binding affinities toward G-quadruplex DNA (*31, 32*). Herein, we examine comparative quadruplex formation, stabilization, and telomerase inhibition by two isomeric symmetrical bisbenzimidazoles, ***p*-Phenbbim** and ***m*-Phenbbim**, which are devoid of any substitution at the aromatic core (Figure 1). The molecule ***p*-Phenbbim** is based on 1,4-substituted symmetrical phenylene bisbenzimidazole which differs in shape from its 1,3-substituted counterpart (***m*-Phenbbim**). Earlier reports suggest that 1,4-substituted phenylene bisbenzimidazole analogues (*33, 34*) may

* To whom correspondence should be addressed. Also J. C. Bose Fellow, Department of Science & Techonology (DST), New Delhi. E-mail: sb@orgchem.iisc.ernet.in, Phone: (91)-80-22932664; Fax: (91)-80-2360-0529.

† Indian Institute of Science.

‡ Jawaharlal Nehru Centre for Advanced Scientific Research.

10.1021/bc9003298 
Published on Web 06/10/2010

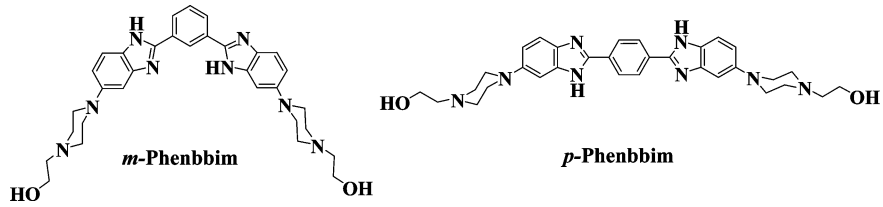


**Figure 1.** Chemical structures of ***m*-Phenbbim** and ***p*-Phenbbim**.

also have affinity toward quadruplex structures. So, we have decided to compare the quadruplex recognition properties of these two isomeric molecules.

In this study, we have utilized telomeric oligonucleotide $d[T_2G_4]_4$ related to the sequence *Tetrahymena thermophilia*, which is capable of forming both intramolecular and intermolecular conformations stabilized by either $K^+$ or $Na^+$ ions. This sequence was shown to exhibit an interesting range of structural polymorphism depending on whether the G-quadruplex was formed in the presence of either $K^+$ or $Na^+$ ions (*30, 35–38*). We discuss comparative G-quadruplex formation, stabilization, and structural alteration of $d[T_2G_4]_4$ quadruplex in the presence of either isomeric compound. We have also reported here the relative efficiencies to inhibit the telomerase activity as indicated by the TRAP[1]assay.

## EXPERIMENTAL SECTION

All starting compounds were procured from Sigma, Aldrich, or E-Merck. All solvents were from Merck, and they were distilled and/or dried prior to use whenever necessary.

**General Spectrometric Characterizations.** NMR spectra were recorded on a Bruker AMX (300 or 400 MHz) spectrometer. IR spectra were recorded on an FTIR Perkin-Elmer Spectrum GX spectrometer. Mass spectra were recorded on a Micromass Q-TOF Micro TM spectrometer.

**5-(4-(2-Hydroxyethyl)-1-piperazinyl)-2-nitroaniline (1).** 5-Chloro-2-nitroaniline (2 g, 11.6 mmol) was taken in dry DMF (5 mL). To this, 1-(2-hydroxyethyl)-piperazine (1.8 g, 13.8 mmol) and $K_2CO_3$ (2.5 g, 18 mmol) were added. It was then heated at 110 °C for 12 h until TLC showed the disappearance of 5-chloro-2-nitroaniline. The crude compound was suspended in water, and the product was extracted with ethyl acetate. The organic layer was washed twice with water, dried over anhydrous $Na_2SO_4$, and concentrated to get 5-(4-(2-hydroxyethyl)-1-piperazinyl)-2-nitroaniline, which was purified by column chromatography using neutral alumina with a solvent system of increasing polarity from $CHCl_3$ to 2% MeOH in $CHCl_3$. The pure product was isolated as a bright yellow solid (2.7 g, 90% yield). $^1$H NMR (300 MHz, $CDCl_3$) $\delta$ ppm = 2.59−2.65 (m, 6H), 3.7 (t, 2H), 3.8 (t, 4H), 5.95 (d, $J$ = 2.7 Hz, 1H), 6.1 (bs, 2H, $NH_2$), 6.29 (dd, $J$ = 9.3, $J$ = 2.7, 1H), 8.02 (d, $J$ = 9.3, 1H).

**5-(4-(2-Hydroxyethyl)-1-piperazinyl)-1,2-phenylenediamine (2).** Compound **1** (0.2 g, 0.66 mmol) was added to a stirred suspension of 10% Pd−C (50 mg) in methanol. The mixture was then stirred at room temperature for 24 h under $H_2$ at 1 atm pressure. It was then filtered and evaporated to get **2** and put for the next step without further purification.

**2,2′-(1,4-Phenylene)-bis-[5-(4-(2-hydroxyethyl)-1-piperazinyl)-1*H*-benzimidazole] (*p*-Phenbbim).** To a methanolic solution of **2** (380 mg, 1.6 mmol), 15 mL of nitrobenzene and 0.5 equiv of 1,4-benzene dialdehyde **5** (115 mg, 0.8 mmol) were added. The resulting solution was heated at 65 °C for 1 h when a bright red precipitate appeared. After cooling the reaction mixture to room temperature, the precipitate was filtered and washed with methanol. The precipitate was subsequently taken in dry nitrobenzene and heated at 150 °C for 3 h. The reaction mixture was cooled and the product precipitated out upon addition of petroleum ether. A yellow solid so obtained was washed repeatedly with petroleum ether until TLC confirmed 100% purity of the material. This was then dried to obtain 370 mg of ***p*-Phenbbim** in 70% yield. FTIR (KBr) ($\nu$ cm$^{-1}$): 3488, 3455, 3054, 2925.6, 1614, 1492, 1440 cm$^{-1}$. $^1$H NMR ($C_{32}H_{38}N_8O_2$.HCl) (400 MHz, DMSO-$d_6$) $\delta$ ppm: 3.37 (t, 4H), 3.80 (bs, 4H), 3.99 (t, 8H), 3.42 (t, 8H), 7.37 (bs, 2H), 7.47 (dd, $J$ = 9.1 Hz, $J$ = 1.96 Hz, 2H), 7.78 (d, 2H, $J$ = 9.1), 8.42 (s, 4H). $^{13}$C NMR (DMSO-$d_6$) $\delta$ ppm: 45.56, 50.94, 54.23, 57.36, 98.47, 113.9, 117.75, 126.13, 127.74, 132.78, 145.91, 148.88. MALDI-TOF: 568.3129 (found), 568.3196 (calcd. for $[M + H]^+$. Elemental Analysis: calcd. For $C_{32}H_{38}N_8O_2 \cdot 1.5\ H_2O$: C, 64.7; H, 6.9; N, 18.8. Found: C, 64.6; H, 6.5; N, 18.5.

**Benzene-1,3-dicarboxaldehyde (4).** α,α′-Dichloro-*m*-xylene **3** (970 mg, 5.54 mmol) and hexamethylenetetramine (1.55 g, 11.08 mmol) were dissolved separately in dry $CHCl_3$ (20 mL), and the mixture was refluxed for 3 h. A white precipitate, which resulted in the salt formation, was filtered and dried. The salt was dissolved in 25 mL water and refluxed for 4 h. The reaction mixture was filtered when hot and the filtrate was cooled in an ice bath, which resulted in the separation of white crystals. It was filtered, washed with cold water, and then dried to get pure aldehyde **4** (370 mg, 50%). $^1$H NMR (300 MHz, $CDCl_3$) $\delta$ ppm: 7.74 (t, 1H), 8.27 (d, $J$ = 7.8 Hz, 2H), 8.39 (s, 1H), 10.13 (s, 2H). FTIR (KBr) ($\nu$ cm$^{-1}$) = 1686 (C=O str.).

**2,2′-(1,3-Phenylene)-bis-[5-(4-(2-hydroxyethyl)-1-piperazinyl)-1*H*-benzimidazole] (*m*-Phenbbim).** To a methanolic solution of **2** (350 mg, 1.5 mmol), 15 mL of nitrobenzene and 0.5 equiv of benzene-1,3-dicarboxaldehyde (100 mg, 0.74 mmol) were added, and the mixture was refluxed for 1 h. A yellow precipitate formed, which was filtered and suspended in nitrobenzene (6 mL) and heated at 150 °C for 3 h. The reaction mixture was cooled to rt, and petroleum ether was added to precipitate out the product as a yellow−green solid. The precipitate was repeatedly washed with petroleum ether to remove nitrobenzene to get 100 mg of the pure compound as judged by TLC (50% yield). IR: 3490, 3458, 3053.5, 2927, 1619, 1450, 1436 cm$^{-1}$. $^1$H NMR (300 MHz, $CD_3OD$): $\delta$ 2.7 (t, 4H), 2.8 (t, 8H), 3.28 (t, 8H), 3.75 (t, 4H), 7.08 (d, $J$ = 8.1 Hz, 2H), 7.64−7.74 (m, 3H), 8.15 (d, $J$ = 8.1), 8.25 (d, $J$ = 9.0 Hz, 2H), 8.5 (s, 1H). $^{13}$C NMR (DMSO-$d_6$) $\delta$ ppm: 45.27, 48.57, 53.71, 56.76, 98.36, 113.74, 116.63, 124.67, 125.52, 126.63, 129.70, 132.90, 146.30, 147.96. MALDI-TOF: 568.3214 (found), 568.3196 (calcd. for $[M + H]^+$). Elemental Analysis: calcd. for $C_{32}H_{38}N_8O_2 \cdot 1.5\ H_2O$: C, 64.7; H, 6.9; N, 18.8. Found: C, 64.4; H 6.8; N, 18.5.

**Oligonucleotides.** HPLC purified oligodeoxyribonucleotides (ODN) $d[T_2G_4]_4$ and $dT_{20}$ were purchased from Sigma Genosys, Bangalore. Their purity was confirmed using high-resolution sequencing gel. The molar concentration of each ODN was determined from absorbance measurements at 260

[1]Abbreviations: hTERT, telomerase reverse transcriptase; DMSO-$d_6$, dimethyl sulfoxide (deuterated); HRMS, high-resolution mass spectrometry; CD, circular dichroic spectropolarimetry; PAGE, polyacrylamide gel electrophoresis; $T_{20}$, 5′-TTT TTT TTT TTT TTT TTT TT-3′; MD, molecular dynamics simulation; TRAP, telomerase repeat amplification protocol.

nm based on their molar extinction coefficients ($\varepsilon_{260}$) 229 000 and 148 400, respectively, for d[$T_2G_4$]$_4$ and d $T_{20}$ markers.

**Quadruplex Formation.** For quadruplex formation from 5′-$T_2G_4T_2G_4T_2G_4T_2G_4$-3′, the following technique was used: the oligonucleotide in buffer (10 mM Tris-HCl at pH = 7.4, 0.1 mM EDTA, and 100 mM NaCl or 100 mM KCl) was heated at 95 °C for 10 min and then snap-chilled, after which the ligands were added in appropriate proportions and incubated at 37 °C for 24 h. To form a quadruplex in the absence of ligands, the same procedure was followed, but the compounds were not added prior to incubation. To check secondary structure formation in the absence of $Na^+$ or $K^+$, again the same technique was followed but the buffer contained no NaCl or KCl.

**Circular Dichroism.** CD spectra were recorded on a JASCO J-810 spectropolarimeter at a scan speed of 50 nm/min and over the wavelength range 220−400 nm. The samples were taken in quartz cuvettes of 1 cm path-length. CD spectra of quadruplex formed in the presence of ligands (at [DNA]:[ligand] ratios = 1:1, 1:2, 1:4) in buffer (10 mM Tris−HCl, pH = 7.4, 0.1 mM EDTA) containing 100 mM NaCl were measured. For another series of experiments, the compounds were titrated into preformed $Na^+$-induced DNA quadruplex in buffer. Between each drug addition, an interval of 20 min was allowed. For experiments carried out in the absence monovalent cations, the compounds were titrated into single-stranded 5′-$T_2G_4T_2G_4T_2G_4T_2G_4$-3′ in buffer, not containing NaCl or KCl. The concentration of DNA was maintained at 2 $\mu$M in all cases. CD melting for uncomplexed and complexed quadruplex (2 $\mu$M) was examined at 295 nm with 1 °C/min ramp.

**Melting Temperature Measurements.** The stability of G-quadruplex DNA was measured by examining the melting temperature ($T_m$) of the folded structures. $T_m$ measurements were performed by following the change in absorbance at 295 nm as a function of temperature. Experiments were carried out in quartz cuvettes stoppered with Teflon caps on a Beckman model 640 spectrophotometer attached with a programmable temperature controller. Concentration of DNA was kept at 2 $\mu$M. Uncomplexed DNA quadruplex and quadruplex structure formed in the presence of ligand molecules were investigated. Samples were heated at the rate of 1.0 °C/min and the absorbance recorded for every 1.0 °C rise in sample temperature. The melting temperatures ($T_m$) were determined from a first derivative analysis of the heating scans.

**Absorption Titration Experiments.** Binding assays were performed with preformed d[$T_2G_4$]$_4$ quadruplex in 10 mM Tris−HCl, having 100 mM KCl and 0.1 mM EDTA buffer, and with d[(5′-$CGT_{13}GC$-3′)/(5′-$GCA_{13}CG$-3′)] duplex in 10 mM Tris−HCl, having 100 mM NaCl and 0.1 mM EDTA buffer at pH 7.4. Ligand solution (50 $\mu$M, 500 $\mu$L) was titrated by stepwise addition of aliquots of DNA solution (4 $\mu$M). After each addition, the mixture was incubated at 25 °C for 15 min before measurement. The fractional decrease in absorbance at 325 nm for each [DNA]/[ligand] ratio was normalized using

$$\Delta A = (A_{free} - A)/(A_{free} - A_{sat})$$

where $A_{free}$ and $A_{sat}$ are the absorbances for the free and fully bound (saturated) ligands. The fraction of bound drug $\alpha$ (on a 0−1 scale) at each intermediate titration position is given directly by the relative $\Delta A$ hypochromicity term (*39*). The concentration of free ligand has been calculated using

$$C_f = (1 - \alpha)C$$

where $C$ is the total ligand concentration (fixed at 50 $\mu$M) and can be used to determine the binding ratio $r$, defined as $(C - C_f)$/[DNA]. Titration data were cast into the form of Scatchard plots of $r/C_f$ versus $r$ for analysis where $K_D$ is the intrinsic equilibrium binding constant and $n$ is an exclusion parameter that defines the number of ligand molecules bound per DNA quadruplex. Data were also fitted using the simpler, linear Scatchard equation

$$r/C_f = K_a(n - r) \quad (1)$$

**Native Gel Electrophoresis.** The single-stranded d[$T_2G_4$]$_4$ and d$T_{20}$ marker (10 pmol/$\mu$L each) were 5′-$^{32}$P labeled using [$\gamma$-$^{32}$P]-ATP (Amersham) using protocol given by the supplier, and purified by chromatography on Sephadex G-50. For G-quadruplex constructs, labeled DNA (10 000 CPM tracer) mixed with unlabeled single-stranded DNA to a concentration of 5 $\mu$M (20 $\mu$L reaction volume) containing 100 mM NaCl, Tris, and 1 mM EDTA buffer, pH 7.4. Resulting solution was heated at 95 °C for 10 min and then snap-chilled after which the individual ligands was added in appropriate quantities and incubated at 37 °C for 24 h. Finally, the ligand incubation with DNA was terminated by the addition of 5 $\mu$L gel loading buffer (30% glycerol, 0.1% bromophenol blue, and 0.1% xylene cyanol). Ten microliters of the subsequent ligand−quadruplex complexes were analyzed on a 12% native PAGE (the gel was pre-run for 30 min). Electrophoresis was carried out for 3 h at 4 °C using 80 V in 0.5× TBE buffer (pH = 7.4) containing 20 mM NaCl. Gels were dried and then visualized on a phosphor imager.

**Computational Methods.** All calculations were performed using the *Gaussian 03* suite program (*40*). Each conformer of the two isomers was optimized at B3LYP/6-31G* level of theory. For each system studied, vibrational frequency calculations were carried out to confirm that they converged to true minima. The Mulliken atomic charges of the optimized ligands obtained from the calculation used for docking studies. The distance (Å) for the all conformers of each isomer was calculated, which is essential for understanding the drug−DNA interaction.

Docking studies were performed using the *AUTODOCK 4.0* program (*41*). Using ADT, nonpolar hydrogens of telomeric G-quadruplex were merged to their corresponding carbons and atomic charges were assigned (*42*). The nonpolar hydrogens of the ligands were merged, and rotatable bonds were assigned. The intramolecular G-quadruplex structure was used as an input for the AUTOGRID program. AUTOGRID performed a precalculated atomic affinity grid map for each atom type in the ligand plus an electrostatics map and a separate desolvation map present in the molecule. The dimensions of the active site box that was placed at the center of the macromolecule were set to 110 Å × 110 Å × 110 Å with a grid spacing of 0.375 Å. Docking calculations were carried out using the Lamarckian genetic algorithm (LGA). Initially, we used a population of random individuals (population size: 150), a maximum number of 2 500 000 energy evaluations, a maximum number of generations of 27 000, and a mutation rate of 0.02. Fifty independent docking runs were done for each ligand. The resulting positions were performed according to a root-mean-square criterion of 0.5 Å.

Molecular dynamics simulations were performed using the sander module of the *AMBER 9.0* program suite and the nucleic acids studied were as treated using the parm99 parameters (*43*). Partial atomic charges for the ligand molecules were derived using the HF/6-31G* basis set followed by RESP calculation, while force-field parameters

were taken from the generalized Amber force field (GAFF) (*44*) using the ANTECHAMBER module. $K^+$ radius was kept at 2.025 Å (*45, 46*). Periodic boundary conditions were applied with the particle-mesh Ewald (PME) method (*47*) used to treat long-range electrostatic interactions. The quadruplex and ligand complexes were solvated in a rectangular box of TIP3P (*48*), water molecules with solvent layers 10 Å and the potassium counterions were added to neutralize the complexes. The hydrogen bonds were constrained using SHAKE (*49*). For the nonbonded interactions, a residue-based cutoff of 10 Å was used. The solvated structures were subjected to initial minimization to equilibrate the solvent and counter cations. The system was then heated from 0 to 300 K in a 100 ps simulation and followed by a 100 ps simulation to the equilibrate the density of the system. Afterward, constant pressure MD simulation of 8 ns was then performed in an NPT ensemble at 1 atm and 300 K. The output and trajectory files were saved every 0.1 and 1 ps for the subsequent analysis, respectively. All trajectory analysis was done with the Ptraj module in the *AMBER 9.0* suite and examined visually using the VMD software package (*50*).

**Telomerase Inhibition.** An aliquot of $5 \times 10^6$ A549 (human lung carcinoma cell line) cells in exponential phase of growth was pelleted and lysed for 30 min on ice using 200 $\mu$L of 1 $\times$ CHAPS lysis buffer (10 mM Tris-HCl, pH 7.5, 1 mM $MgCl_2$, 1 mM EGTA, 0.1 mM benzamidine, 5 mM $\beta$-mercaptoetanol, 0.5% CHAPS 10% glycerol in 8200 $\mu$L volume). The lysate was centrifuged at 12 000 rpm for 30 min at 4 °C and the supernatant collected, stored at −80 °C, and used as the telomerase source. Telomerase activity was assayed using a modified telomere repeat amplification protocol (TRAP) assay. Briefly, an appropriate primer TS (5′-AATCCGTC-GAGCAGAGTT-3′) has been 5′-labeled with [$\gamma$-$^{32}$P]-ATP and T4 polynucleotide kinase. After enzyme inactivation (85 °C for 5 min), a 120 $\mu$L TRAP reaction mix (50 $\mu$M of dNTPs, 0.2 $\mu$g of labeled TS, 0.1 $\mu$g of return primer ACX, 500 ng of protein extract, 2 U *Taq* polymerase) was prepared in the presence/absence of increasing drug concentration in 20 mM Tris-HCl pH 8.3, 68 mM KCl, 1.5 mM $MgCl_2$, 1 mM EGTA, 0.05% v/v Tween-20. An internal control template (0.01 mmol TSNT) with its return primer (1 ng) was added to the reaction mixture. Then, the telomerase elongation step has been performed (30 min at 30 °C), followed by a PCR amplification step (30 cycles of 30 s at 94 °C and 30 s at 59 °C). The reaction products were loaded onto a 10% polyacrylamide gel (19:1) in TBE 0.5×. Gels were transferred to Whatman 3 mm paper, dried under vacuum at 80 °C, and read using a Phosphorimager 840 (Amersham). Measurements were made in triplicate with respect to a negative control run using the equivalent TRAP-PCR conditions but omitting the protein extract, thus ensuring that the ladders observed were not due to artifacts of the PCR reaction.

## RESULTS AND DISCUSSION

Owing to the interesting array of structural variations exhibited by the telomeric repeats of *Tetrahymena thermophilia*, we selected the single-stranded telomeric repeat $d[T_2G_4]_4$ as a model G-tract for the present study. The sequence $d[T_2G_4]_4$ has been shown to exhibit a wide range of interesting structural polymorphism depending upon whether quadruplex DNA formation occurs in the presence of $Na^+$ or $K^+$ (*35, 36*). Due to its structural polymorphism, *Tetrahymena* quadruplex has been used as a model system by other researchers also to probe ligand−DNA interactions (*37, 51, 52*). We were interested to compare the interaction of the two new isomeric benzimidazoles with the various structural polymorphs of the quadruplex structure.

The hybrid quadruplex formed in $Na^+$ solution bears a circular dichroism (CD) spectral profile with approximately equal intensity maxima around 295 nm (antiparallel characteristics) and 260 nm (parallel) and a minimum around 237 nm (*35, 53*). In contrast, the mixture of multistranded intermolecular and intramolecular quadruplex species formed in $K^+$ solution was marked by the development of an intense positive band at 265 nm, shoulder at 295 nm, and a minimum around 242 nm (*53*). Among these, the intramolecular quadruplexes are less stable, and their structures may be easily altered by interacting with appropriate ligands or proteins, and so forth.

The benzimidazole nucleus is a constituent of many of the bioactive heterocyclic compounds that are of wide interest

**Scheme 1**[a]

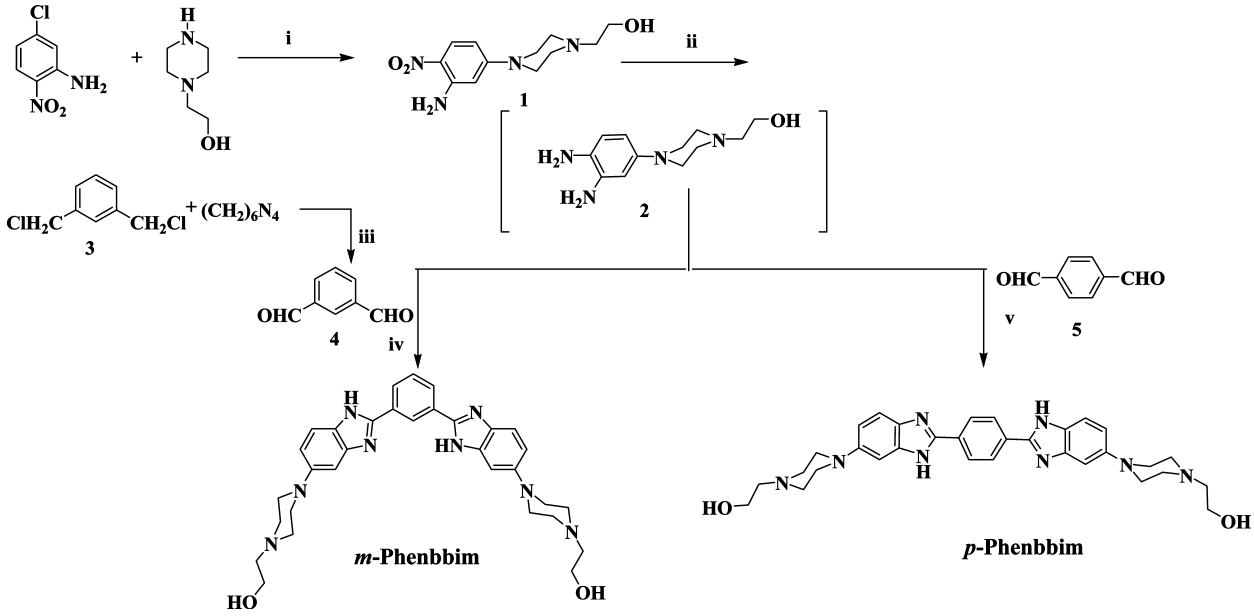


[a] Reagents, conditions, and yields: (i) Anhydrous $K_2CO_3$, dry DMF, 110 °C, 12 h, 90%; (ii) $H_2$ (1 atm), 10% Pd−C, MeOH, rt, 24 h; (iii) dry $CHCl_3$, reflux, 3 h then water, reflux 4 h, 50% (overall); (iv) compound **2**, $PhNO_2$/MeOH, 65 °C, 1 h, then $PhNO_2$, 150 °C, 3 h, 50%; (v) compound **2**, $PhNO_2$/MeOH, 65 °C, 1 h, then $PhNO_2$, 150 °C, 2 h, 70%.

because of their diverse biological and clinical applications (*54*). Moreover, benzimidazoles are structural isosteres of natural nucleotides (purines), which allows them to interact easily with the biopolymers of the living system. Besides having these properties, bisbenzimidazole compounds are known to have cell and nuclear membrane permeability and are being used in cytometry and in nuclear chromosomal staining in cell culture (*55–58*). With these factors taken together, we have synthesized two isomeric bisbenzimidazoles ***p*-Phenbbim** and ***m*-Phenbbim** having central symmetrical and planar core, extended delocalized $\pi$-electron system, and side chain tertiary amines, which will develop positive charge via protonation under physiological conditions (pH = 7.4). These molecules also possess groups that are able to form hydrogen bonds with the DNA bases and phosphate backbone of loops, the properties required for the stabilization of G-quadruplex structure (*57, 58*).

**Synthesis.** For the synthesis of the bisbenzimidazoles, commercially available 5-chloro-2-nitroaniline was chosen as the key starting material. It was reacted with 1-(2-hydroxyethyl)piperazine to produce compound **1**. The next step involved catalytic hydrogenation of **1** over 10% Pd−C to afford the diamine **2**. Subsequent oxidative condensation of **2** with 1,3- or 1,4-benzene-dicarboxaldehydes afforded the required ***m*-** and ***p*-Phenbbim**, respectively, in good yields (Scheme 1).

**Circular Dichroism Spectroscopy.** To investigate the ability of the above molecules toward the stabilization of G-quadruplex structure, quadruplex DNA formation was explored in the presence of ***m*-Phenbbim** and ***p*-Phenbbim**, at [DNA]:[compound] ratios of 1:1, 1:2, and 1:4, in buffer containing 100 mM NaCl. CD spectral data showed that preincubation with ***p*-Phenbbim** formed a structure in which the characteristic CD signatures of a $Na^+$-stabilized quadruplex, i.e., two positive maxima at 295 and 260 nm, respectively, were retained (*35*). However, there was a hypochromism of both the bands implying some kind of interaction between ***p*-Phenbbim** and G-quadruplex (Figure 2A).

With ***m*-Phenbbim** on the other hand, a very interesting phenomenon was observed. At [DNA]:[drug] ratios 1:1 and 1:2, there was a decrease in the 260 nm CD band along with a concomitant enhancement in the 295 nm band (Figure 2B) However, at [DNA]:[drug] ratio of 1:4, there was a dramatic increase in the 260 nm band along with a red-shift to 265 nm. The intensity of the 295 nm band was reduced; also, the minima at 235 nm became more negative and shifted to 239 nm (Figure 2B).

Next, to examine if ***m*-Phenbbim** could induce such a change in preformed G-quadruplex structure, we first formed a DNA quadruplex in 100 mM NaCl and titrated the molecule against this. As seen in the previous section, up to [DNA]:[drug] ratio 1:2, the 260 nm CD band reduced in intensity and the 295 nm band increased (Supporting Information). At [DNA]:[drug] ratio of ~1:3, there was a dramatic reversal in the CD profile (Supporting Information). The 260 nm band increased in intensity accompanied by a marked red-shift to 265 nm, while the 295 nm band intensity decreased. Finally, at [DNA]:[drug] ratio of 1:6, the 295 nm band appeared as a shoulder to the pronounced 265 nm band. Also, the negative band at 235 nm was red-shifted to 240 nm (Supporting Information). The results were similar to that observed in the previous case where quadruplex structure was formed in the presence of ***m*-Phenbbim**.

Next, we wanted to check the kind of DNA secondary structure these drugs induced in the absence of any added monovalent cations like $Na^+$ or $K^+$. This is important, as

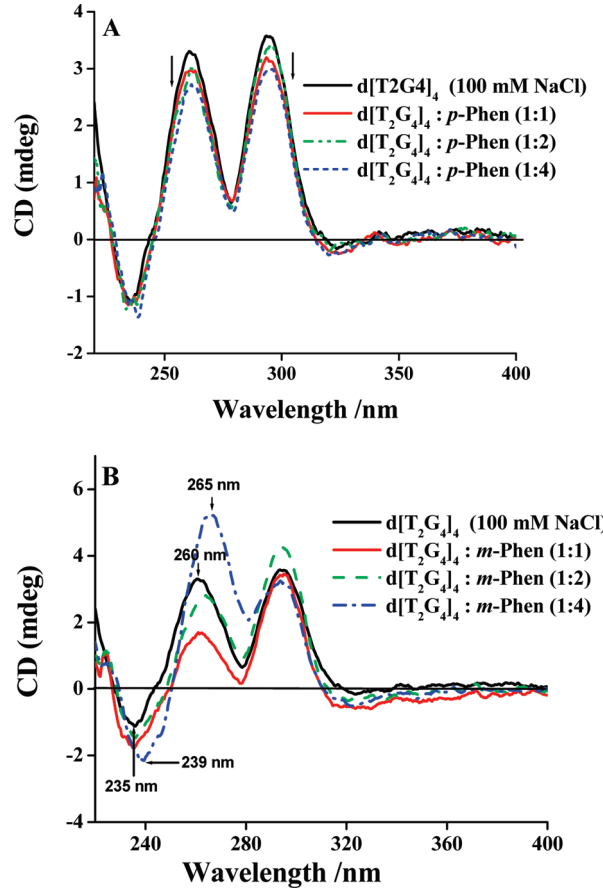


**Figure 2.** CD profile of quadruplex DNA structure formed in buffer containing 100 mM NaCl in the presence of ligands (A) ***p*-Phenbbim** and (B) ***m*-Phenbbim**, at [DNA]/[Drug] ratio of 1:1, 1:2, and 1:4. The DNA concentration was 2 $\mu$m in each case.

only a few ligands are currently known that are capable of inducing the quadruplex formation in the absence of any added cation (*14, 30*). To single-stranded DNA, which had no specific secondary structure (Figure 3, dotted line), compound ***m*-Phenbbim** was titrated. Addition of drug caused a pronounced red-shift of the DNA, i.e., from 256 nm to 265 nm, along with a marked enhancement in the intensity of the said band. Initially, at [DNA]: [drug] = 1:2, there were two bands, one at 265 nm and another, a pronounced hump, at 293 nm. As the drug concentration was increased, the 265 nm maxima increased in intensity and the 293 nm band decreased. The shallow minimum at 235 nm became more intense and shifted to 240 nm. There were two clear isodichroic points at 252 and 282 nm, respectively (Figure 3, solid lines). The final CD signature at [DNA]:[drug] ratio of 1:8 resembled the CD profile of $K^+$-quad (Figure 3B).

Titration of ***p*-Phenbbim** to randomly structured ss-DNA also led to changes in CD signature of DNA, but the changes were different and less pronounced than that observed with ***m*-Phenbbim** (Supporting Information). However, either of the compounds could not cause any structural alterations of the $K^+$-quad (Supporting Information).

Specific secondary structure formation was evident from the development of characteristic CD bands. From the CD signature, a structure similar to that formed in the presence of KCl was interpreted. An important feature was the persistence of isodichroic points at 252 and 282 nm throughout the titration. The presence of these two isodichroic points signifies an equilibrium involving at least two species. Hence, the molecule ***m*-Phenbbim** not only caused structural transition of preformed

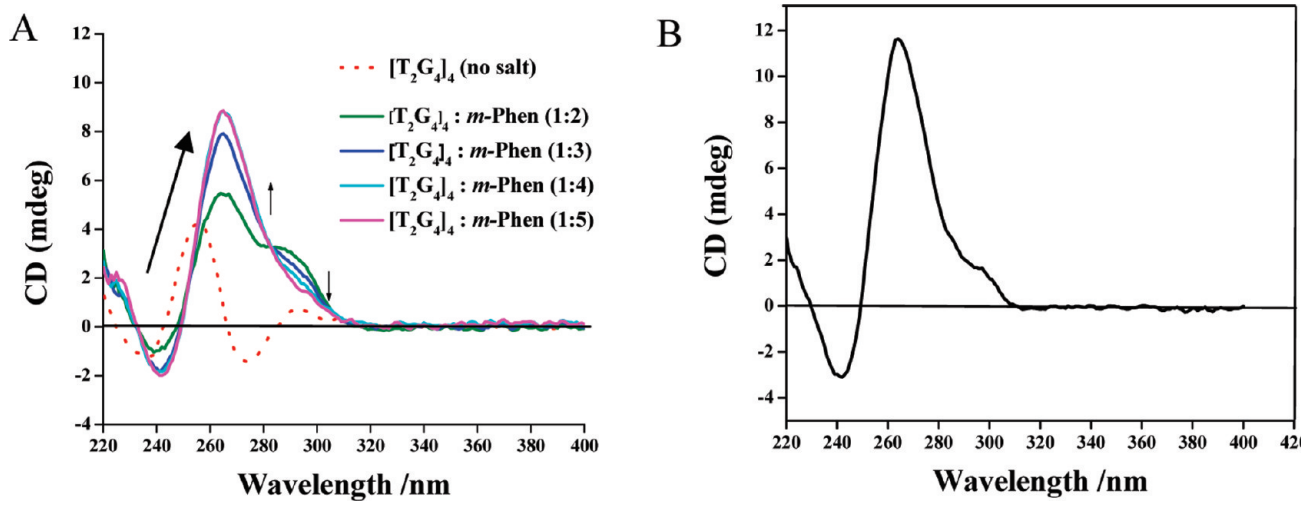


**Figure 3.** (A) Compound ***m*-Phenbbim** titrated into single-stranded d$[T_2G_4]_4$ (2 $\mu$M), in buffer in the absence of KCl or NaCl. The dotted line shows the CD profile of DNA alone. Solid lines show the CD profile of DNA on incremental addition of the compound. Arrows indicate the change in CD bands. (B) The CD profile of quadruplex structure formed in 100 mM KCl.

**Table 1. Melting Temperature ($T_m$) of DNA Quadruplex[a] by Monitoring Absorbance at 295 nm**

| | $T_m$ (°C) | $\Delta T_m$ (°C)[b] |
|---|---|---|
| DNA (buffer) | 53.4 | |
| DNA (buffer)[c] | 36 | |
| DNA + ***p*-Phenbbim** (1:4) | 57.1 | 3.7 |
| DNA + ***m*-Phenbbim** (1:2) | 58.5 | 5.1 |
| DNA + ***m*-Phenbbim**(1:5)[c,d] | 48 | 12 |

[a] Quadruplex (2 $\mu$M strand conc.) formed in buffer (10 mM Tris−HCl at pH = 7.4, 0.1 mM EDTA, and 100 mM NaCl) in the presence of the individual ligands. [b] $\Delta T_m$ values represent the differences in melting temperatures for the ligand-bound and free quadruplex. [c] CD melting in buffer (10 mM sodium cacodylate at pH 7.4, 0.1 mM EDTA, and 100 mM LiCl), for DNA alone at 295 nm. [d] CD melting in buffer for ligand-bound complex at 265 nm.

$Na^+$ stabilized quadruplex, but also induced secondary structure formation from a randomly structured single-stranded DNA in the absence of any monovalent cation.

**Melting Temperature Measurements ($T_m$).** Melting of intramolecular quadruplex structure was accompanied by a hypochromicity of the 295 nm absorption band (*15*). Thermal denaturation of the quadruplex, formed in the presence of 100 mM NaCl, showed hypochromicity of the 295 nm absorption band. Next, the melting of secondary structures formed in the presence of the two compounds in 100 mM NaCl buffer was examined. The molecule ***p*-Phenbbim**, at various [DNA]:[drug] ratios (1:1, 1:2, and 1:4), induced stabilization of the intramolecular quadruplex structure. Reversible melting profiles were obtained when the absorption at 295 nm *vs.* temperature was monitored (Supporting Information, only the heating scans are shown). With ***m*-Phenbbim**, at [DNA]:[drug] ratio 1:2, secondary structure dissociation was accompanied by a hypochromism of the 295 nm absorption band, and heating/cooling profiles were almost reversible (Supporting Information).

From the CD titrations and thermal melting data, it is apparent that ***p*-Phenbbim**, at all concentrations, stabilizes $Na^+$-induced intramolecular quadruplex structure without causing any major structural changes in the latter. The melting temperature enhancement of the drug-bound quadruplex (compared to the uncomplexed quadruplex) indicates stabilization of the DNA secondary structure by the molecule (Table 1).

On the other hand, ***m*-Phenbbim** retained the intramolecular $Na^+$-induced quadruplex structure only at low concentrations. However, at higher drug concentrations a dramatic reversal of the DNA CD profile occurred and at [DNA]:[***m*-Phenbbim**] of ~1:8, the DNA CD signatures resembled that of $K^+$-quad, with an intense positive band at 265 nm, a shoulder at 290 nm, and a negative peak at 240 nm. When the drug was titrated into preformed $Na^+$-quad, similar structural transition was observed, and at [drug]/[DNA] ratios of ≥4:1, the CD signatures resembled that of a $K^+$-quad. The most dramatic results were seen when the drug was titrated into single-stranded d$[T_2G_4]_4$ in the absence of $K^+$ or $Na^+$ in buffer. Compound ***p*-Phenbbim** provided weaker stabilization to the quadruplex than ***m*-Phenbbim**.

Quadruplex has a positive CD signal at 295 nm, which is intensified after interacting with the added compounds. We performed CD melting at 295 nm to again confirm the effect of ligand on the stability of quadruplex and to rule out any confusion in the results obtained from UV melting experiments. At [DNA]:[drug] ratio 1:5, ***m*-Phenbbim** gave a stabilization of 12 °C (Figure 4) ($T_m$ for quadruplex alone at 295 nm was 36 °C, and with ligand, it was 48 °C) in 10 mM sodium cacodylate buffer having 100 mM LiCl (Supporting Information) ($Li^+$ is known to help the formation of quadruplex but does not stabilize it) (*61*). Hence ***m*-Phenbbim** have high affinity for the quadruplex DNA.

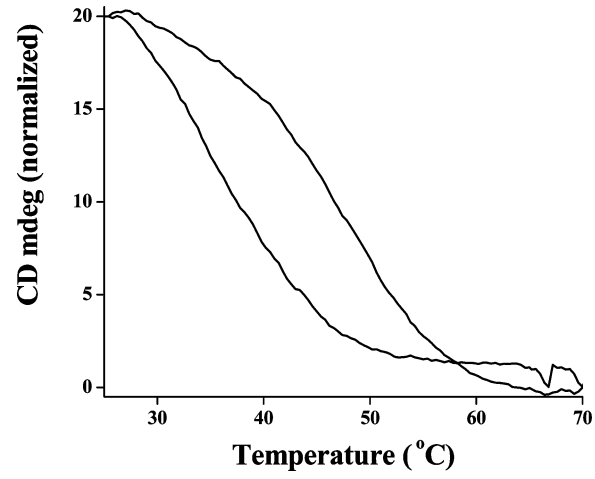


**Figure 4.** Normalized CD melting profiles of *Tetrahymena* d$[T_2G_4]_4$ quadruplex (2 $\mu$M strand conc.) in LiCl buffer (10 mM sodium cacodylate having 100 mM LiCl) at 295 nm and with 10 $\mu$M of ***m*-Phenbbim**.

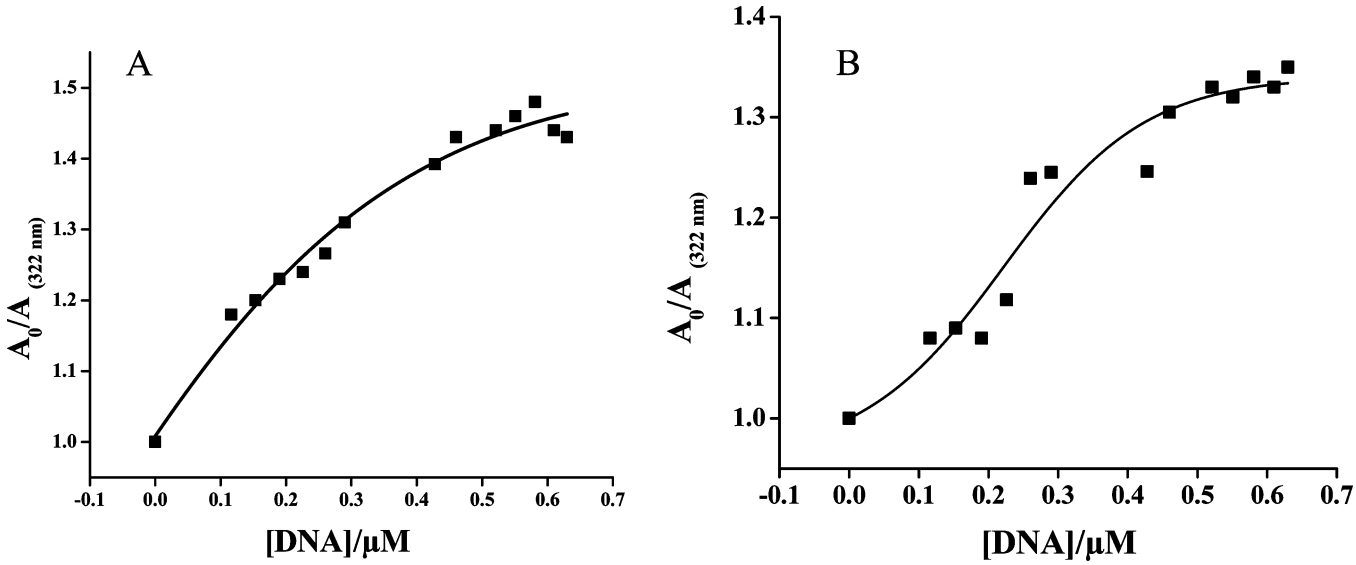


**Figure 5.** UV−vis titration of ***m*-Phenbbim** (A) and ***p*-Phenbbim** (B) upon addition of preformed G-quadruplex DNA in 10 mM Tris-HCl, 100 mM KCl, and 0.1 mM EDTA buffer solution at pH = 7.4. The saturation plot obtained upon plotting $A_0/A$ against [DNA] expressed in base molarity change.

**Table 2. Dissociation Constant ($K_D$) of *m*-Phenbbim and *p*-Phenbbim to Preformed *Tetrahymena* Quadruplex Sequence in 100 mM KCl Buffer and [(5′-CGT$_{13}$GC-3′)/(5′-GCA$_{13}$CG-3′)] Duplex[a]**

| | $K_D$ ($10^5$ $M^{-1}$) | |
|---|---|---|
| ligand | d[$T_2G_4$]$_4$ | duplex |
| ***m*-Phenbbim** | 4.22 ± 0.8 | 0.058 ± 0.03 |
| ***p*-Phenbbim** | 1.76 ± 0.6 | 0.089 ± 0.12 |
| **berberine** | 5.64 ± 0.3 | 0.12 ± 0.03 |

[a] Binding assays were performed with preformed d($T_2G_4$)$_4$ quadruplex in 10 mM Tris-HCl, having 100 mM KCl and 0.1 mM EDTA buffer, and with [(5′-CGT$_{13}$GC-3′)/(5′-GCA$_{13}$CG-3′)] duplex in 10 mM Tris-HCl, having 100 mM NaCl and 0.1 mM EDTA buffer at pH 7.4.

The UV−vis titration spectra of both ***m*-Phenbbim** and ***p*-Phenbbim** were preformed with G-quadruplex in 100 mM KCl solution (Figure 5A,B), which resulted in hypochromicity, indicating a specific binding and strong stacking interaction between either ligands and G-quadruplex DNA. The UV−vis titration results were converted into Scatchard plots (Supporting Information), and the dissociation constants ($K_D$) were determined by linear fitting. Compound ***m*-Phenbbim** binds to the G-quadruplex DNA showing a dissociation constant ($K_D$) of $4.22 \times 10^5$ $M^{-1}$, while ***p*-Phenbbim** presents a relatively lower binding constant with a $K_D$ of $1.76 \times 10^5$ $M^{-1}$ (Table 2). The natural product berberine binds with G-quadruplex DNA with a binding constant $K_D$ of $5.64 \times 10^5$ $M^{-1}$, which is comparable to that of ***m*-Phenbbim**.

**Native Gel Electrophoresis.** Electrophoresis on 12% native polyacrylamide gel showed the emergence of a new band after interaction with ***m*-Phenbbim** and ***p*-Phenbbim** (Figure 6). Compound ***m*-Phenbbim** showed complete conversion at [DNA]:[drug] of ∼1:12, while other isomers could not completely convert at this ratio. A second band also emerged from ***p*-Phenbbim** giving rise to a heterogeneous mixture of electrophoretic bands.

Taken together from the CD titration and electrophoresis data, it appears that ***m*-Phenbbim** is able to convert antiparallel intramolecular quadruplex into parallel intramolecular quadruplex. An intermolecular structure formation would cause even greater retardation in the electrophoretic mobility. Indeed, a similar observation was reported with human telomeric sequence when quadruplex was formed in the presence of PEG (*62*). These authors proposed the conversion from hybrid structure to parallel propeller structure. ***p*-Phenbbim** also induces similar topological conversion but only at higher [drug]:[DNA] ratio. In our case, both original quadruplex band and the band emerging after interaction with the compounds had significantly higher mobility than that of the $T_{20}$ marker. It is well-documented that the intramolecular quadruplex formed by the sequence d[$T_2G_4$]$_4$ (in $K^+$ solution) has mobility corresponding to the $T_{15}$ marker. Hence, our results unambiguously indicate that the difference in mobility of the drug−DNA complex is due to the change in the topology of the quadruplex after interacting with the compound and not due to any aggregation. Compound ***m*-Phenbbim** thus converts the hybrid intramolecular quadruplex into a parallel-stranded intramolecular quadruplex more efficiently than its linear isomer, ***p*-Phenbbim**.

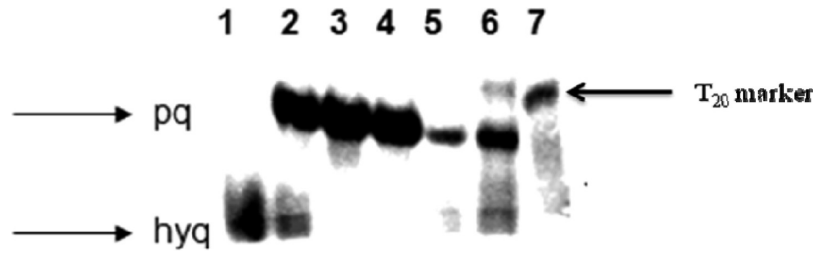


**Figure 6.** Electrophoresis of *Tetrahymena* d[$T_2G_4$]$_4$ quadruplex with ligands in 100 mM NaCl. Lane 1: 5 μM strand. Lanes 2, 3, and 4: 5 μM strand +30, 40, and 60 μM of ***m*-Phenbbim**. Lanes 5 and 6: 5 μM strand +30 and 60 μM ***p*-Phenbbim**. Lane 7: $T_{20}$ marker. The notation "hyq" means hybrid intramolecular quadruplex and "pq" means parallel intramolecular quadruplex.

**Molecular Modeling Studies.** To gain more understanding on the nature of interactions that prevail between bisbenzimidazole derivatives with the telomeric G-quadruplex, an approach that combined a molecular docking and MD simulations were performed. The solution structure of *Tetrahymena* $d[T_2G_4]_4$ G-quadruplex in $Na^+$ solution is already known on the basis of NMR (PDB-186D) studies, which indicates that this sequence adopts a unique folding topology. Molecular docking studies were first carried out to predict the possible interactions between the ligand and G-quadruplex DNA. It has been previously shown that G-quadruplex binders can stack on the surface of the G-quartet planes. It was not possible to dock the ligands on the G-quartet planes because these were covered with loops. Interaction energies would be much lower if the ligands could be docked between G-quartet plane and loop of the quadruplex DNA. While the molecule ***p*-Phenbbim** has a linear-shaped central aromatic core, ***m*-Phenbbim** consists of a V-shaped central aromatic core. The end-to-end length of the central core of ***m*-Phenbbim** as calculated from energy-minimized calculation is 19.89 Å (Supporting Information), which is almost equal to the distances (20.18 Å; Supporting Information) of one of the grooves of the *Tetrahymena* G-quadruplex parallel structure. The molecular organization of the central core (internal H-bonds) and electronic/electrostatic properties (two benzimidazole system and piparazine side arms) make ***m*-Phenbbim** perfectly fit for the recognition of the quadruplex target. On the other hand, for the linear ***p*-Phenbbim** the end-to-end length is almost 23 Å, which is considerably longer than the length of the groove (Supporting Information). The interaction energy (free energy, $\Delta G$) and docking energy of ***p*-Phenbbim** with quadruplex DNA were found to be higher than that of ***m*-Phenbbim** (Supporting Information). This again suggests that, while both compounds could stabilize G-quadruplex DNA, but ***m*-Phenbbim** provides more stabilization to the G-quadruplex DNA than ***p*-Phenbbim**.

On the other hand, the X-ray-crystal structure of *Oxytricha nova* telomeric quadruplex (PDB 3EM2) has similar sequence to that of *Tetrahymena* G-quadruplex. Here, each quadruplex contains two strands of the sequence d[5′-GGGGTTTTGGGG-3′] with a diagonal fold topology, in which the thymine loops are lying diagonally across the top and bottom of the stack of the guanine quartets and strands of each sequence are antiparallel to each other. The quadruplex shows an alternating syn−anti arrangement of guanine glycosidic torsion angles along the strand and syn−syn and anti−anti arrangement within the quartet. One base in each of the terminal quartet is slightly more tilted than the others. This stacks effectively with the 3′-thymine residue from the loop. The diagonal topology of the structure results in one wide, two medium, and one narrow groove (*63*).

A close examination of the crystal structure of 22AG (1KF1, RCSB Protein Data Bank) shows that a G-quartet can be considered a square aromatic surface whose dimensions (13.6 Å and 10.9 Å) are closely related to that of the conformation ***m*-Phenbbim** (Supporting Information Figure S9; Table 4), which indicates good coplanarity of the molecule with G-quartet plane, and hence, this could explain the high stabilization properties of quadruplex by this ligand. Using Autodock, we have docked our two ligands in between G-quartet plane and T4 loop of *Oxytricha nova* telomeric quadruplex DNA. On the basis of the docking results, MD simulation (8 ns) were performed on the two complexes formed by G-quadruplex DNA (*Oxytricha nova*) with ligands ***m*-Phenbbim** and ***p*-Phenbbim** in the binding mode of intercalation between G-quartet and T4 loop. All of the models were quite stable during the dynamics runs. During the simulation runs, it has been found that the complex with ***m*-Phenbbim** was giving much lower rmsd than the complex with ***p*-Phenbbim** (Figure 7). It also has been found that due to the V-shape and bond flexibility of the ***m*-Phenbbim** ligand two positively charged side chains are going toward the groove and forming strong hydrogen bonding with the phosphate backbone and $NH_2$ hydrogen of the guanine residue (Figure 7). Recently, a crystal structure of BRACO-19 with bimolecular human quadruplex has been published showing the binding of the side chains of the compounds in the grooves of the quadruplex DNA (*64*). The molecular organization of the central core (internal H-bonds) and $\pi$-stacking interaction (3.4 Å) and electronic/electrostatic properties (two benzimidazole system and piparazine side arms) make derivatives perfectly fitted for the recognition of the quadruplex target.

For ***m*-Phenbbim** at higher [drug]/[DNA] ratio of >10:1, we indeed observe an induced CD signal (ICD) possibly due to groove binding (Supporting Information). On the other hand, due to the linear shape of ***p*-Phenbbim** its side chains were not properly fitted in the grooves. This again suggests that, while both compounds could stabilize G-quadruplex DNA, ***m*-Phenbbim** provides more stabilization to the G-quadruplex DNA than ***p*-Phenbbim**.

One problem encountered during G-quadruplex recognition may be the interference caused by duplex DNA when compounds are injected *in vivo*. Intercalation and minor groove binding are the two possible binding modes with duplex DNA. Intercalators are known to increase the viscosity of DNA solution (*29*). Viscometric titrations with CT DNA indicate that ***m*-Phenbbim** is a considerably poorer intercalator than ethidium bromide (EtBr) (Table 5, Supporting Information). It also shows a very low increment in the melting temperature ($T_m$) of CT-DNA when compared with that of a classical minor groove binder Hoechst-33258 (Table 5, Supporting Information) indicating its insignificant affinity toward duplex DNA at drug:DNA ratio of 0.5. This observation is consistent with a report in which a structural analogue of ***m*-Phenbbim** was shown to have very low affinity with duplex DNA as compared to Hoechst 33258 (*28*). Hence, ***m*-Phenbbim** has weak binding with duplex DNA in either mode (intercalation or minor groove binding), and it has significant quadruplex affinity, as suggested by CD titrations and thermal denaturation experiments.

**Telomerase Inhibition (TRAP assay).** Finally, we have examined the telomerase inhibition ability of these two compounds. In this paper, we have presented the binding studies with a nonhuman quadruplex DNA sequence (*Tetrahymena*). At the same time, it is of interest to examine whether these ligands may also work as possible anticancer agents. Indeed, several potential quadruplex ligands, e.g., porphyrins (TMPyP4), telomestatin, BRACO 19, and so forth, which inhibit the enzyme telomerase in telomerase repeat amplification protocol (TRAP) assay, also demonstrate antitumor activity (*17, 65, 66*). The modified TRAP assay provides an estimate of the telomerase inhibition by small molecules (*67*). Accordingly, as a first step both of the compounds have been tested using TRAP assay at concentrations ranging from 2.5 $\mu$M to 30 $\mu$M. Compound ***m*-Phenbbim** inhibited telomerase activity at 10 $\mu$M concentration; on the other hand, for ***p*-Phenbbim** there was no significant inhibition of the telomerase activity even at 30 $\mu$M (Figure 8). These results indicate that ***m*-Phenbbim** may have higher affinity toward the G-quadruplex structures

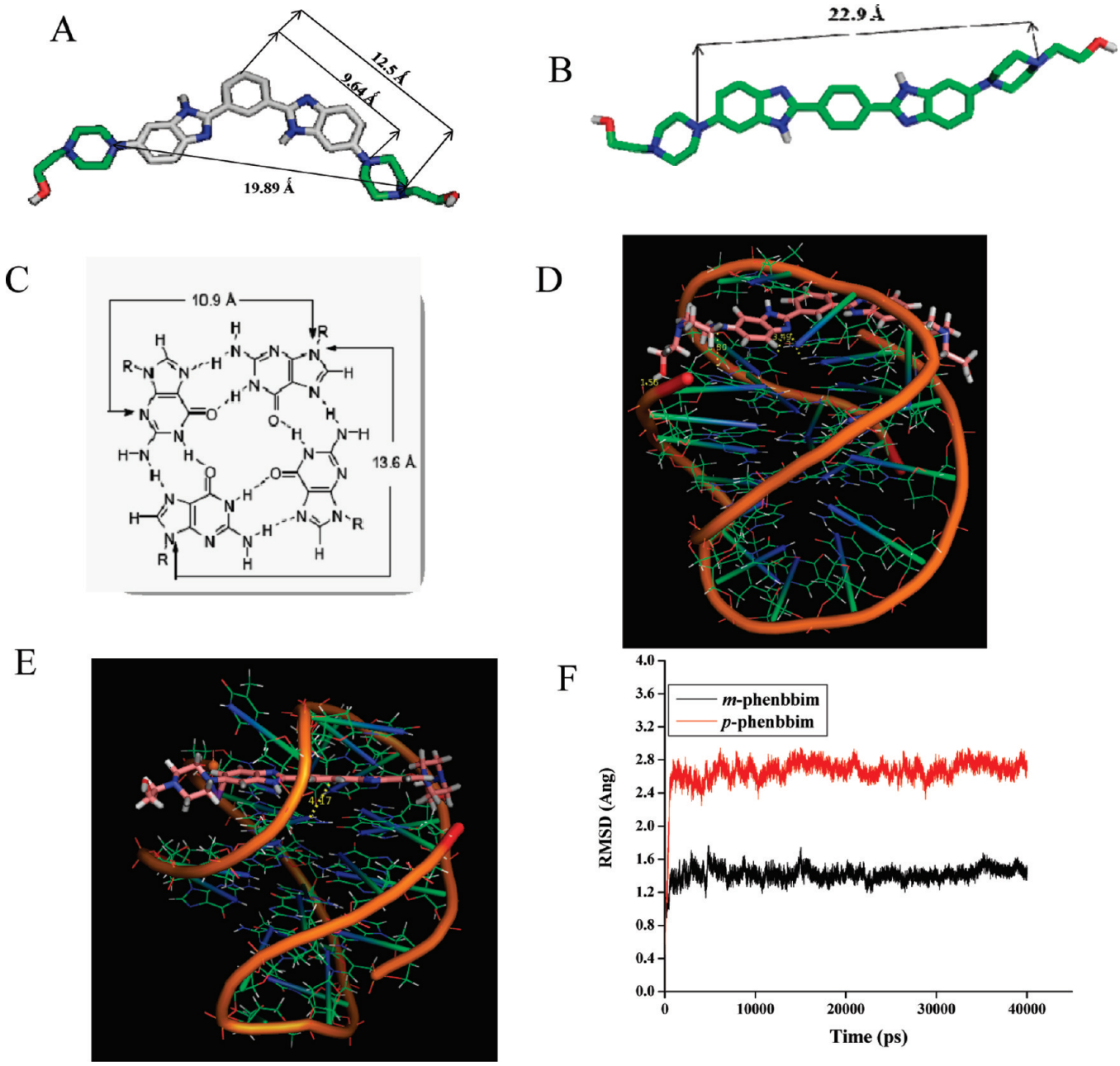


**Figure 7.** (A,B) Optimized structures at the B3LYP/6-31G* level of theory of ***m*-Phenbbim** and ***p*-Phenbbim**, respectively. (C) Structures of the G-tetrad; model of ligand−quadruplex complex. (D,E) ***m*-Phenbbim** stacking on the surface of G-quartet (D) and ***p*-Phenbbim** stacking on the surface of G-quartet (E). (F) Plots following the stability of the models during the dynamics runs (rmsd plots with time).

formed by human telomeric DNA sequence than its counterpart ***p*-Phenbbim**.

## CONCLUSION

In summary, we have developed two new isomeric bisbenzimidazole-based compounds, both showing stabilization of the G-quadruplex DNA structure. The affinity of the compounds toward the G-quadruplex is dependent on the shape of the molecule. While the linear isomer stabilized the $Na^+$-induced intramolecular quadruplex, the other (V-shaped) isomer caused a remarkable structural transition of the latter above a certain threshold ligand concentration. The latter also showed higher affinity toward the G-quadruplex. The final CD signature of DNA and retardation on 12% native acrylamide gel suggested possible switching of antiparallel intramolecular quadruplex into intramolecular parallel quadruplex. Interestingly, even in the absence of any monovalent cation like $Na^+$ or $K^+$, the same isomer induced specific secondary structure formation from randomly oriented single-stranded DNA.

Compound ***m*-Phenbbim** has comparable molecular size and geometry to that of the G-quartet, and hence, it could stack over three guanine residues of the quartet and thus provides high stabilization (comparable to that of natural quadruplex stabilizing ligand berberine) of the quadruplex and induce structural switching, while, being linear, ***p*-Phenbbim** could stack only with two guanine residues of the quartet. The differential interaction of the two isomers with the quadruplex DNA forming sequence opens up interesting possibilities where drug−DNA recognition can be fine-tuned by minor alteration of the molecular structure of the ligand. Finally, there are only a few examples known

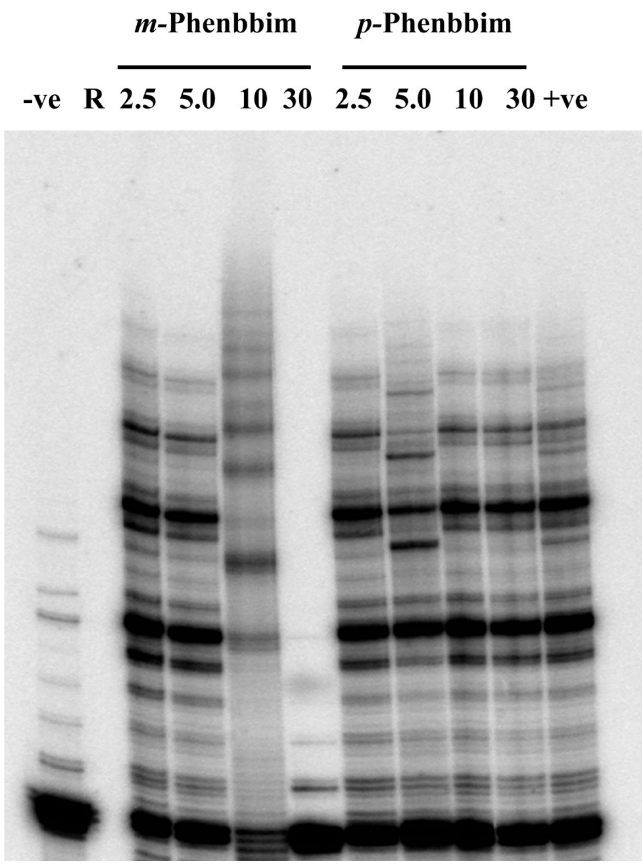


**Figure 8.** Representative experiments for the determination of telomerase inhibitory properties by the bisbenzimidazole derivatives. TRAP assay performed with increasing concentrations of ***m*-Phenbbim** and ***p*-Phenbbim**. Lane 1: (−) *ve* control (absence of enzyme and drug). Lane 2: R = PCR control. Lane 3, 4, 5, and 6: TRAP reaction mixture + (2.5, 5, 10, and 30 $\mu$M of ***m*-Phenbbim**). Lanes 7, 8, 9, and 10: TRAP reaction mixture + (2.5, 5, 10, and 30 $\mu$M of ***p*-Phenbbim**). Lane 11: (+) *ve* control (absence of drug).

where a small organic molecule has been shown to induce quadruplex DNA formation from randomly oriented single-stranded DNA in the absence of other mono- or divalent cations. The TRAP experiment further demonstrated that the *m*-isomer is highly active toward telomerase activity.

## ACKNOWLEDGMENT

This work was supported by a grant from Department of Science and Technology, New Delhi, India. AKJ is thankful to DBT for a Postdoctoral Fellowship.

**Supporting Information Available:** CD titrations other than those given in the manuscript, calculations on gas-phase conformation and effects of salvation, schematic representation of molecular staking on G-quartet and interatomic distances, docking structure and energies, comparison of duplex binding properties of ***m*-Phenbbim**. This material is available free of charge via the Internet at http://pubs.acs.org.

## LITERATURE CITED

(1) Blackburn, E. H. (1991) Structure and function of telomeres. *Nature 350*, 569–573.
(2) Harley, C. B., Futcher, A. B., and Greider, C. W. (1990) Telomeres shorten during ageing of human fibroblasts. *Nature 345*, 458–460.
(3) Gowan, S. M., Harrison, J. R., Patterson, Valenti, L. M., Read, M. A., Neidle, S., and Kelland, L. R. (2002) A G-quadruplex-interactive potent small-molecule inhibitor of telomerase exhibiting in vitro and in vivo antitumor activity. *Mol. Pharmacol. 61*, 1154–1162.
(4) Cech, T. R. (2000) Life at the end of the chromosome: Telomeres and telomerase. *Angew. Chem. Int. Ed. 39*, 34–43.
(5) Kerwin, S. M. (2000) G-quadruplex DNA as a target for drug design. *Curr. Pharmacol. Des. 6*, 441–478.
(6) Perry, P. J., and Kell, L. R. (1998) Telomeres and telomerase: targets for cancer chemotherapy. *Exp. Opin. Ther. Patents 8*, 1567–1586.
(7) Franceschin, M. (2009) G-Quadruplex DNA structures and organic chemistry: More than one connection. *Eur. J. Org. Chem.* 2225–2238.
(8) Kim, M. Y., Vankayalapati, H., Shin-Ya, K., Wierzba, K., and Hurley, L. H. (2002) Telomestatin, a potent telomerase inhibitor that interacts quite specifically with the human telomeric intramolecular G-quadruplex. *J. Am. Chem. Soc. 124*, 2098–2099.
(9) Barbieri, C. M., Srinivasan, A. R., Rzuczek, S. G., Rice, J. E., LaVoie, E. J., and Pilch, D. S. (2007) Defending the mode, energetic and specificity with which a macrocyclic hexaoxazole binds to human telomeric G-quadruplex DNA. *Nucleic Acids Res. 35*, 3272–3286.
(10) Hurley, L. H. (2002) DNA and its associated processes as targets for cancer therapy. *Nat. Rev. Cancer 2*, 188–200.
(11) Pindur, U., and Fischer, G. A. (1996) DNA complexing minor groove-binding ligands: Antitumour and antimicrobial drug design. *Curr. Med. Chem. 3*, 379–406.
(12) Phillips, K., Dauter, Z., Murchie, A. I. H., Lilley, D. M. J., and Luisi, B. (1997) The crystal structure of a parallel-stranded guanine tetraplex at 0.95 Å resolution. *J. Mol. Biol. 273*, 171–182.
(13) Tang, C. F., and Shafer, R. H. (2006) Engineering the quadruplex fold: Nucleoside conformation determines both folding topology and molecularity in guanine quadruplexes. *J. Am. Chem. Soc. 128*, 5966–5973.
(14) Rodriguez, R., Pantos, G. D., Goncalvs, D. P. N., Sanders, J. K. M., and Balasubramanian, S. (2007) Ligand induced-driven G-quadruplex conformational switching by using an unusual mode of interaction. *Angew. Chem. Int. Ed. 46*, 5405–5407.
(15) Mergny, J. L., Phan, A. T., and Lacroix, L. (1998) Following G-quartet formation by UV-spectroscopy. *FEBS Lett. 435*, 74–78.
(16) Han, H., and Hurley, L. H. (2000) G-quadruplex DNA: A potential target for anti-cancer drug design. *Trends Pharmacol. Sci. 21*, 136–141.
(17) Burger, A. M., Schultes, Dai, F., Reszka, C. M., Moore, A. P., Double, J. A., and Neidle, S. (2005) The G-Quadruplex-interactive molecule BRACO-19 inhibits tumour growth, consistent with telomere targeting and interference with telomerase function. *Cancer Res. 65*, 1489–1496.
(18) Moorehouse, A. D., Santos, A. M., Gunaratnam, M., Moore, M., Neidle, S., and Mosses, J. E. (2006) Stabilization of G-quadruplex DNA by highly selective ligands via click chemistry. *J. Am. Chem. Soc. 128*, 15972–15973.
(19) Dash, J., Shirude, P. S., and Balasubramanian, S. (2008) Quadruplex recognition by bis-indole carboxamides. *Chem. Commun.* 3055–3057.
(20) Li, G., Huang, J., Zhang, M., Zhou, Y., Zhang, D., Wu, Z., Wang, S., Weng, X., and Zhou, X. Y. (2008) G. Bis(benzimidazole)pyridine derivative as a new class of G-quadruplex inducing and stabilizing ligand. *Chem. Commun.* 4564–4566.
(21) Monchaud, D., Yang, P., Lacroix, L., Teulade-Fichou, M. P., and Mergny, J. L. (2008) A metal-mediated conformational switch controls G-quadruplex binding affinity. *Angew. Chem., Int. Ed. 47*, 4858–4861.
(22) Bhattacharya, S., and Thomas, M. (2000) Facile synthesis of oligopeptide distmycin analogs devoid of hydogen bond donors or acceptors at the N-terminus: Sequence-specific duplex DNA binding as a function of peptide chain length. *Tetrahedron Lett. 41*, 5571–5575.
(23) Thomas, M., Varshney, U., and Bhattacharya, S. (2002) Distamycin analogs without leading amide at their N-termini

comparative binding properties to AT- and GC-rich DNA sequences. *Eur. J. Org. Chem.* 3604–3615.

(24) Ghosh, S., Defrancq, E., Lhomme, J. H., Dumy, P., and Bhattacharya, S. (2004) Efficient conjugation and characterization of distamycin based peptides with selected oligonucleotide stretches. *Bioconjugate Chem. 15*, 520–529.

(25) Bhattacharya, S., and Mandal, S. S. (1995) Ambient oxygen activating water soluble cobalt-salen complex for DNA cleavage. *J. Chem. Soc. Chem. Commun.* 2489–2490.

(26) Mandal, S. S., Kumar, N. V., Varshney, U., and Bhattacharya, S. (1996) Metal-ion dependent oxidative DNA cleavage by transition metal complex of a new water soluble salen derivative. *J. Inorg. Biochem. 63*, 265–272.

(27) Bhattacharya, S., and Mandal, S. S. (1996) DNA cleavage by intercalatable cobalt-bispicolylamine complexes activated by visible light. *Chem. Commun.* 1515–1516.

(28) Mandal, S. S., Varshney, U., and Bhattacharya, S. (1997) Role of central metal ion and ligand charge in the DNA binding and modification by metallosalen complexes. *Bioconjugate Chem. 8*, 798–812.

(29) Chaudhuri, P., Majumder, H. K., and Bhattacharya, S. (2007) Synthesis, DNA binding, and *Leishmania* topoisomerase inhibition activities of a novel series of anthra[1, 2*d*]imidazole-6,11-dione derivatives. *J. Med. Chem. 50*, 2536–2540.

(30) Jain, A. K., Reddy, V. V., Paul, A., Muniyappa, K., and Bhattacharya, S. (2009) Synthesis and evaluation of a novel class of G-quadruplex-stabilizing small molecules based on the 1,3-phenylene-bis(piperazinyl benzimidazole) system. *Biochemistry 48*, 10693–10704.

(31) Drewe, W. C., Nanjunda, R., Gunaratnam, M., Beltran, M., Parkinson, G. N., Reszka, A. P., Wilson, D., and Neidle, S. (2008) Rational design of substituted diarylureas: A scaffold for binding to G-quadruplex motifs. *J. Med. Chem. 51*, 7751–7767.

(32) Muller, S., Pantos, G. D., Rodriguez, R., and Balasubramanian, S. (2009) Controlled-folding of a small molecule modulates DNA G-quadruplex recognition. *Chem. Commun.* 80–82.

(33) Bathini, Y., Rao, K. E., Shea, R. G., and Lown, W. (1990) Molecular recognition between ligands and nucleic acids: novel pyridine- and benzoxazole-containing agents related to Hoechst 33258 that exhibit altered DNA sequence specificity deduced from footprinting analysis and spectroscopic studies. *Chem. Res. Toxicol. 3*, 268–280.

(34) Hori, Y., Bichenkova, E. V., Wilton, A. N., El-Attug, M. N., Sadat-Ebrahimi, S., Tanaka, T., Kikuchi, Y., Araki, M., Sugiura, Y., and Douglas, K. T. (2001) Synthetic inhibitors of the processing of pretransfer RNA by the ribonuclease P ribozyme: Enzyme inhibitors which act by binding to substrate. *Biochemistry 40*, 603–608.

(35) Hardin, C. C., Henderson, E., Watson, T., and Prosser, J. K. (1991) Monovalent cation induced structural transitions in telomeric DNAs: G-DNA folding intermediates. *Biochemistry 30*, 4460–4472.

(36) Chen, F. M. (1992) Strontium ($2^+$) facilitates intermolecular G-quadruplex formation of telomeric sequences. *Biochemistry 31*, 3769–3776.

(37) Murashima, Sakiyama, T. D., Miyoshi, D., Kuriyama, M., Yamada, T., Miyazawa, T. and, and Sugimoto, N. (2008) Cationic porphyrin induced a telomeric DNA to G-quadruplex form in water. *Bioinorg. Chem. Appl.* 1–5.

(38) Wang, Y., and Patel, D. J. (1994) Solution structure of the *Tetrahymena* telomeric repeat d $(T_2G_4)_4$ G-tetraplex. *Structure 2*, 1141–1156.

(39) Peacocke, A. R., and Skerrett, J. N. H. (1956) The interaction of aminoacridines with nucleic acids. *J. Chem. Soc., Faraday Trans. 52*, 261–279.

(40) Frisch, M. J., Trucks, G. W., Schlegel, H. B., Scuseria, G. E., Robb, M. A., Cheeseman, J. R., Montgomery, J. A., Vreven, T., Kudin, K. N., Burant, J. C., and Milliam, J. M. *Gaussian 03*, Gaussian, Inc., Wallingford, CT.

(41) Morris, G. M., Goodsell, D. S., Halliday, R. S., Huey, R., Hart, W. E., Belew, R. K., and Olson, A. J. (1998) Automated docking using a Lamarckian genetic algorithm and an empirical binding free energy function. *J. Comput. Chem. 19*, 1639–1662.

(42) Sanner, M. F. (1999) Python: a programming language for software integration and development. *J. Mol. Graph. Model. 17*, 57–61.

(43) Cornell, W. D., Cieplak, P., Bayly, C. I., Gould, I. R., Merz, K. M., Jr., Ferguson, D. M., Spellmeyer, D. C., Fox, T., Caldwell, J. W., and Kollman, P. A. (1995) A second generation force field for the simulation of proteins, nucleic acids, and organic molecules. *J. Am. Chem. Soc. 117*, 5179–5197.

(44) Wang, J., Wolf, R. M., Caldwell, J. W., Kollman, P. A., and Case, D. A. (2004) Development and testing of a general Amber force field. *J. Comput. Chem. 25*, 1157–1174.

(45) Hazel, P., Huppert, J., Balasubramanian, S., and Neidle, S. (2004) Loop-length-dependent folding of G-quadruplex. *J. Am. Chem. Soc. 126*, 16405–16415.

(46) Hazel, P., Parkinson, G. N., and Neidle, S. (2006) Predictive modelling of topology and loop variations in dimeric DNA quadruplex structures. *Nucleic Acids Res. 34*, 2117–2127.

(47) Darden, T., York, D., and Pedersen, L. (1993) Particle mesh Ewald: an $N \log(N)$ method for Ewald sums in large systems. *J. Chem. Phys. 98*, 10089–10092.

(48) Jorgensen, W. L., Chandrasekhar, J., Madura, J. D., Impey, R. W., and Klein, M. L. (1983) Comparison of simple potential functions for simulating liquid water. *J. Chem. Phys. 79*, 926–935.

(49) Ryckaert, J. P., Ciccotti, G., and Berendsen, H. J. C. (1977) Numerical integration of the Cartesian equations of motion of a system with constraints: molecular dynamics of *n*-alkanes. *J. Comput. Phys. 23*, 327–41.

(50) Humphrey, W., Dalke, A., and Schulten, K. (1996) VMD: visual molecular dynamics. *J. Mol. Graph. 14*, 33–8, plates 27−28.

(51) Pagano, B., Virno, A., Mattia, C. A., Mayol, L., Randazzo, A., and Giancola, C. (2008) Targeting DNA quadruplexes with distamycin A and its derivatives: An ITC and NMR study. *Biochimie 90*, 1224–1232.

(52) Wei, C., Lihua, Wang, L., Jia, G., Jun, Z. J., Han, G., and Li, C. (2009) The binding mode of porphyrins with cation side arms to $(TG_4T)_4$ G-quadruplex: Spectroscopic evidence. *Biophys. Chem. 143*, 79–84.

(53) Rezler, E. M., Seenisamy, J., Bashyam, J. S., Kim, M. Y., White, E., Wilson, W. D., and Hurley, L. H. (2005) Telomestatin and diseleno sapphyrin bind selectively to two different forms of the human telomeric G-quadruplex structure. *J. Am. Chem. Soc. 127*, 9439–9447.

(54) Bhattacharya, S., and Chaudhuri, P. (2008) Medical implications of benzimidazole derivatives as drugs designed for targeting DNA and DNA associated processes. *Curr. Med. Chem. 15*, 1762–1777.

(55) Stokke, T., and Steen, H. B. (1985) Multiple binding modes for Hoechst 33258 to DNA. *J. Histochem. Cytochem. 33*, 333–338.

(56) Latt, S. A., and Wohlleb, J. C. (1975) Optical studies of the interaction of 33258 Hoechst with DNA, chromatin, and metaphase chromosomes. *Chromosoma 52*, 297–316.

(57) Chaudhuri, P., Ganguly, B., and Bhattacharya, S. (2007) An experimental and computational analysis on the differential role of the positional isomers of symmetric bis-2-(pyridyl)-1*H*-benzimidazoles as DNA binding agents. *J. Org. Chem. 72*, 1912–1923.

(58) Tawar, U., Jain, A. K., Dwarakanath, B. S., Chandra, R., Singh, Y., Chaudhury, N. K., Khaitan, D., and Tandon, V. (2003) Influence of phenyl ring disubstitution on bisbenzimidazole and terbenzimidazole cytotoxicity: synthesis and biological evaluation as radioprotectors. *J. Med. Chem. 46*, 3785–3792.

(59) Kieltyka, R., Fakhoury, J., Moitessier, N., and Sleiman, H. F. (2008) Platinum phenanthroimidazole complexes as G-quadruplex DNA selective binders. *Chem.—Eur. J. 14*, 1145–1154.

(60) Arora, A., Balasubramanian, C., Kumar, N., Agrawal, S., Ojha, R. P., and Maiti, S. (2008) Binding of berberine to human telomeric quadruplex - spectroscopic, calorimetric and molecular modeling studies. *FEBS J. 275*, 3971–3983.

(61) De. Cian, A., Guittat, L., Kaiser, M., Sacca, B., Amrane, S., Bourdoncle, A., Albrtti, P., Teulade-Fichou, M. P., Lacriox, L., and Mergny, J. L. (2007) Fluorescence-based melting assays for studying quadruplex ligands. *Methods 42*, 183−195.

(62) Xue, Y., Kan, Z. Y., Wang, Q., Yao, Y., Liu, J., Hao, Y.-H., and Tan, Z. (2007) Human telomeric DNA forms parallel-stranded intramolecular G-quadruplex in $K^+$ solution under molecular crowding condition. *J. Am. Chem. Soc. 129*, 11185–11191.

(63) Haider, S. M., Parkinson, G. N., and Neidle, S. (2003) Structure of a G-quadruplex-ligand complex. *J. Mol. Biol. 326*, 117–125.

(64) Campbell, N. H., Parkinson, G. N., Reszka, A. P., and Neidle, S. (2008) Structural basis of DNA quadruplex recognition by an acridine drug. *J. Am. Chem. Soc. 130*, 6722–6724.

(65) Gomez, D., Aouali, N., Renaud, A., Douarre, Ce.-T., Shinya, K., Tazi, J., Martinez, S., Trentesaux, C., Morjani, H., and ois Riou, J.-F. (2003) Resistance to senescence induction and telomere shortening by a G-quadruplex ligand inhibitor of telomerase. *Cancer Res. 63*, 6149–6153.

(66) Mikami-Terao, Y., Akiyama, M., Yuza, Y., Yanagisawa, T., Yamada, O., and Yamada, H. (2008) Antitumor activity of G-quadruplex-interactive agent TMPyP4 in K562 leukemic cells. *Cancer Lett. 261*, 226–234.

(67) Read, M. J., Gunaratnam, M., Beltran, A. P., Reszka, R. V., and Neidle, S. (2008) TRAP-LIG, a modified telomere repeat amplification protocol assay to quantitate telomerase inhibition by small molecules. *Anal. Biochem. 380*, 99–105.

BC9003298